

RSC Advances



This is an *Accepted Manuscript*, which has been through the Royal Society of Chemistry peer review process and has been accepted for publication.

Accepted Manuscripts are published online shortly after acceptance, before technical editing, formatting and proof reading. Using this free service, authors can make their results available to the community, in citable form, before we publish the edited article. This *Accepted Manuscript* will be replaced by the edited, formatted and paginated article as soon as this is available.

You can find more information about *Accepted Manuscripts* in the [Information for Authors](#).

Please note that technical editing may introduce minor changes to the text and/or graphics, which may alter content. The journal's standard [Terms & Conditions](#) and the [Ethical guidelines](#) still apply. In no event shall the Royal Society of Chemistry be held responsible for any errors or omissions in this *Accepted Manuscript* or any consequences arising from the use of any information it contains.



Journal Name

ARTICLE

A role of oxygen adsorption and gas sensing mechanism for cerium vanadate (CeVO₄) nanorods

Jimin Hou,^a Huihan Huang,^a Zhizhong Han^b and Haibo Pan^{*ac}Received 00th January 20xx,
Accepted 00th January 20xx

DOI: 10.1039/x0xx00000x

www.rsc.org/

CeVO₄ nanorods (NRs) were successfully synthesized via a one step hydrothermal method in the case of disodium edentate (EDTA) as a chelating agent. CeVO₄ NRs are assigned to the zircon type tetragonal structure and exhibited pure single-crystal as determined through the XRD analysis. FE-SEM images indicate that the as-prepared samples present as square-section nanorod, and the length and sectional size of CeVO₄ NRs are ~ 1.5 μm and ~ 100 nm, respectively. Further, HRTEM images and SAED diffraction pattern confirm that the main exposed surfaces of CeVO₄ NRs is (010) and (004) lattice plane with high exposed percentage (ca. 96.77%) around NRs and the growth direction is along the (200) lattice plane. The CeVO₄ NRs presents pure phase, no other impurity phases from the FTIR and Raman spectroscopy. XPS results indicate that the vanadium atoms on the surface remained with mixture valence states, *i.e.*, pentavalent state (V⁵⁺) and trivalent state (V³⁺) as dangling bonds around oxygen vacancies induced by EDTA desorption during hydrothermal process. An acetone gas sensor based on CeVO₄ NRs was fabricated and exhibits significant response (0.5 s) and recovery (80 s) with high selectivity at the optimum working temperature (108 °C). This is mainly due to the presence of trivalent state (V³⁺) served as the active sites, which provide a large number of oxygen vacancies (V_o) identified by XPS and infrared experiment at 300 ppm O₂ (0.003 atm). Further, it demonstrates that the response to acetone for the gas sensor is crucially dependent on the adsorbed oxygen (O_{ads}) on (010) or (004) facets of CeVO₄ NRs, where the redox reaction with acetone occurred reversibly.

Introduction

Many rare earth vanadates had been studied because of their outstanding optical, electrical and magnetic properties, and had been widely used in sensors, tribology and heat-resistant materials.¹ Rare earth orthovanadates (ReVO₄) such as cerium vanadate (CeVO₄) are important semiconducting derivatives of the vanadium oxides due to their useful electronic and catalytic properties for electrochromic materials and gas sensors.² Especially, CeVO₄ has also shown excellent redox nature and optical properties because of particular 4f electronic structure and diverse electronic transition mode of rare earth elements.^{3,4} As a consequence, the design and synthesis of CeVO₄ nanostructures with well-defined size and morphology had attracted much attention.^{5,6} Luo *et al.* prepared the nanorods-assembled CeVO₄ hollow spheres by a simple hydrothermal synthesis method for oxidative dehydrogenation of propane as an active catalyst.⁷ In the gas sensing field, earlier, hydrothermally synthesized CeVO₄ and CeO₂-CeVO₄ nanopowders were investigated as ethanol sensors, and the gas sensor by using CeVO₄ nanopowders performed poorly even at high temperature (400 °C).⁸ In addition, a kind of CeVO₄ nanorods (NRs) with highly selective ethanol sensing properties were synthesized by a one step hydrothermal method, while the synthesis process was much more complicated and V₂O₅ phase presented yet.⁹ And so far, they have rarely been studied for the detection of acetone molecule. Note that

the redox reactions occur mainly at active sites for gas sensing materials, and a larger specific surface area can provide more active sites. Thus, reasonable controlling the hierarchical morphology of CeVO₄ nanomaterials with high specific surface area will effectively improve the gas-sensing properties. As for gas sensing mechanism, as reported, the gas response was inferred according to the oxygen vacancies and adsorbed oxygen on the sensing layer. However, these behaviours were not still identified by experiment.¹⁰

Acetone has been widely applied in medical, pesticide and paint industries, and used as solvent, reagent, and extractant.¹¹ When emitted, it is harmful to the environment and humans. Slight irritation of noses, throats, lungs and eyes in the presence of 300–500 ppm acetone has been reported.^{12,13} Once exposing to 2000 ppm acetone environment, human suffer nausea and vomiting symptoms.¹⁴ Acetone is also a flammable gas with lower explosive limit (LEL) and upper explosive limit (UEL) of 2.6 and 12.8%, respectively.¹⁵ Hence, analyzing the concentration of acetone in the environment is very important to our health and industrial safety.¹⁴ Zhou *et al.* prepared the highly sensitive acetone gas sensor based on porous ZnFe₂O₄ nanospheres by annealing the precursor, which was synthesized via a simple template-free solvothermal route with ethanol/ethylene glycol (EG) binary solvents.¹⁶ Do *et al.* prepared the conductimetric acetone gas sensor by using polypyrrole and polyaniline conducting polymers with chemical oxidation-casting (COC), chemical vapour deposition (CVD) and impregnated oxidation (IO) techniques.¹⁵

In the present work, we successfully synthesized the CeVO₄ NRs via a one step hydrothermal method and applied disodium edentate (EDTA) as surfactant to control the shape synthesis by maintaining pH ~ 9.5 using sodium hydroxide solution. Various characterizations were carried out to obtain the crystal structure and morphological information of the as-prepared samples. Furthermore, in order to demonstrate the potential applications, the resulting CeVO₄ NRs

^a College of Chemistry, Qishan Campus, Fuzhou University, Fuzhou, Fujian 350108, China. E-mail: hbpan@fzu.edu.cn; Telephone: 86-591-22866127; Fax: 86-591-22866127

^b School of Pharmacy, Fujian Medical University, Fuzhou, Fujian 350108, China.

^c Fujian Key Lab of Medical Instrument and Pharmaceutical Technology, Fuzhou University, Fuzhou, Fujian 350002, China

were used to fabricate a gas sensor, which was then tested for response to a variety of gases. The response and selectivity toward acetone for the sensor were researched at the optimal operating temperature. Especially, before using to detect the specific gas, the adsorption by oxygen molecules from air on the surface of CeVO₄ NRs was tried to be identified by an infrared experiment. A surface depletion layer model has also been established to explain the gas sensing mechanism according to the results involving XPS and infrared experiment.

Experimental

Synthesis reagents

The chemical reagents used in the work were cerium acetate [Ce(CH₃CO₂)₃] (Aladdin Co., Ltd.), sodium vanadate (Na₃VO₄) (Aladdin Co., Ltd.), EDTA (Sinopharm Chemical Reagent Co., Ltd.), alcohol (Sinopharm Chemical Reagent Co., Ltd.), acetone (CH₃COCH₃) (Sinopharm Chemical Reagent Co., Ltd.), hydrogen (H₂) (Fuzhou SIA industrial gases Co., Ltd.), and methane (CH₄) (Fuzhou SIA industrial gases Co., Ltd.). All the chemicals were of analytical grade purity and were used as received without further purification.

Synthesis process

The approach for fabricating CeVO₄ samples was as follow. Appropriate amount of Ce(CH₃CO₂)₃ (0.8 mmol) and EDTA (1 mmol) as template were added to distilled water in a 50.0 ml flask, forming a chelated cerium and stirred for several minutes. An amount of stoichiometric Na₃VO₄ solution was added above complex solution. A transparent yellowish solution (60 ml) was obtained. The pH was adjusted to 9.5 using sodium hydroxide solution (4 M). Then, it was transferred into a Teflon-lined stainless-steel autoclave (80 ml) and maintained at 180 °C for 24 h. With the autoclave cooling down to room temperature, the precipitated powders were separated by centrifugation, washed with deionized water and ethanol for several times. Finally, the CeVO₄ nanosized products were dried at 60 °C for further characterization.

Characterization

X-ray diffraction analysis (XRD) was performed using a Rigaku-miniflex II (Rigaku Company, Japan) diffractometer operating with monochromatic Cu Kα₁ (λ = 0.154056 nm) radiation at 30 kV and 15 mA. Data were collected over a 2θ range of 10–80°, with a scan speed of 0.02°/s. Surface morphologies of the samples across the entire substrate were characterized by field-emission scanning electron microscopy (FE-SEM, Hitachi S4800, Hitachi Company, Japan). In order to improve the resolution of the micrographs, the samples were sprayed with Au before SEM measurement. Transmission electron microscopy (TEM) and High-resolution TEM (HRTEM) images were obtained using Tecnai G2 F20 S-TWIN, 200 kV (FEI Company, USA). The samples for HRTEM were obtained by dissolving a small amount of product in ethanol and diluted, and taking a few drops on carbon supported on the copper network, and drying. Raman spectrum was recorded by a confocal Raman microspectrometer (Renishaw, UK) under the excitation of 785 nm diode laser and was collected in a range of 400–1800 cm⁻¹. FTIR spectra of the CeVO₄ NRs mixed with KBr were recorded on a Spectrum-2000 FTIR spectrophotometer (PerkinElmer Corp., USA) in the range of 400–4000cm⁻¹. The surface properties of samples were characterized by X-ray photoelectron spectroscopy (XPS) in a PHI Quantum 2000 Scanning ESCA Microprobe (PHI. Corp., USA)

system with a monochromatic Al Kα_{1,2} source (1,486.60 eV). All binding energies were referenced to the C1s peak at 284.8 eV of the surface adventitious carbon.

Gas sensing measurement

The fabrication process of a gas sensor can be described below. Firstly, CeVO₄ NRs were mixed with an appropriate amount of alcohol to obtain a paste, and then the paste was coated uniformly on the surface of ceramic tube (thickness of about 0.2 mm) under dry in the shade. Finally, a Ni–Cr alloy coil was inserted inside the alumina tube as a heater.¹⁷ After aging for 10 days at 4 V heating voltage, the gas sensing performance of gas sensor was tested with JF02E gas sensor test system (Jinfeng Tech. Co. Ltd., Kunming, China). The tested gases included H₂, CH₄ and CH₃COCH₃. The sensitivity (S) of gas sensor towards testing gases was determined by the relative ration of the resistance variation, $S = (R_0 - R_g)/R_0$ (%), where R₀ is the resistance in air and R_g is the resistance in a testing gas. Response time is defined as the time required for the sensor resistance to reach 90% of the equilibrium value after acetone molecules was injected and recovery time is taken as the time necessary for the gas sensor resistance to reach 90% of the baseline value in air. To identify the performance related with V³⁺, oxygen vacancies and adsorbed oxygen molecules, a low oxygen pressure experiment for CeVO₄ NRs gas sensor was carried out based on the corresponding resistance in air and infrared at 300 ppm O₂ (0.003 atm) with a flowing in O₂-N₂ mixture.

Results and discussion

Characterization of samples

As shown in Fig.1, all of the recorded diffraction peaks are well indexed to the pure tetragonal phase of CeVO₄ with lattice constant of a = b = 7.399 Å and c = 6.496 Å, which is in good consistent with those from the standard JCPDS card NO. 12-0757.¹⁸ In contrast to the diffraction peaks, the growth rate of (200) lattice plane, 2θ = 24.032°, is faster than the other lattice planes. No other impurity phases could be observed.

The morphologies and microstructures of the as-obtained CeVO₄ samples were investigated by FE-SEM (Fig. 2). Fig. 2a shows the low-magnification FE-SEM image of the products as uniform and dispersed square-section nanorods. The high-magnification FE-SEM images of CeVO₄ NRs present in Fig. 2b and c, which reveal detail information of CeVO₄ NRs with sectional width ~ 100 nm and length ~ 1.5 μm (Fig. 2d), corresponding to the tetragonal structure shown in the XRD analysis (Fig. 1). As known, there is no related report that the CeVO₄ NRs were synthesized.

Transmission electron microscopy (TEM) observations and corresponding selected area electron diffraction (SAED) were carried out to reveal additional information concerning the structural and surface properties of the as-prepared samples. From Fig. 3a and c, TEM images of CeVO₄ NRs indicate that the size and shape of the products were in good accordance with the FE-SEM observations throughout their entire lengths and rough surfaces. In fact, the clear lattice fringes in HRTEM image (Fig. 3b) and SAED pattern (the inset in Fig. 3c) demonstrate that the CeVO₄ NRs are of uniform single crystals. The 4.89 Å spacing of crystallographic planes is assigned to the (101) lattice plane of CeVO₄ NRs. It also demonstrates the monocrystalline feature of CeVO₄ materials based on the (101), (004), (200) lattice planes in SAED pattern, corresponding to the HRTEM images. The above results indicate that the main exposed lateral surface of CeVO₄ NRs is (010) and (004) lattice plane and the growth direction of CeVO₄ NRs is mainly along the (200) lattice plane, coinciding with the XRD analysis. Based on the morphology of CeVO₄ NRs (Fig. 2), the exposed

percentage for (010) and (004) plane is ca. 96.77%. However, the growth rate of (010) and (004) lattice plane was inhibited because of the chelation of disodium edentate. Therefore CeVO₄ NRs are with complete lattice shape and present as a nanorod structure with square section after EDTA decomposition during hydrothermal process and washed with deionized water and ethanol, respectively.

In order to monitor the presence of other organic phase and the functional group of CeVO₄ NRs, Raman and FTIR spectrum were characterized in Fig. S1. In Fig. S1a, two main Raman modes are observed at 801 and 863 cm⁻¹, which are assigned to A_{1g} vanadate symmetric stretching (ν_1) and E_g antisymmetric stretching of vanadates (ν_3) of VO₄³⁻, respectively. And in the FTIR spectrum (Fig. S1b), two distinct peaks at 767 and 437 cm⁻¹ are corresponding to stretching vibration of V-O bond¹⁹ and Ce-O bond²⁰, respectively. A smooth linear is observed from 4000-1000 cm⁻¹, which indicates without both impurity phases in CeVO₄ NRs and hydroxide radicals.

In order to research surface nature, XPS was carried out to examine the surface component of the as-prepared samples. Fig. 4a shows XPS survey spectra, indicating the presence of Ce 4p, V 2p, O 1s, V 2s²¹, Ce MNN²² and Ce 3d. And C 1s peak appears due to testing electrodes, confirming the high chemical purity of the CeVO₄ NRs. As to Ce 3d spectrum, two characteristic states, Ce 3d_{5/2} and Ce 3d_{3/2}, presents, assigned to Ce³⁺ valance state (Fig. 4b).^{9,18,22,23} The peaks related with vanadium valence in Fig. 4c and Table 1 correspond to two characteristic states, V 2p_{3/2} and V 2p_{1/2}, assigning to dominant pentavalent state V⁵⁺ and minor trivalent state V³⁺, and the latter is correspond to the dangling bonds of V⁵⁺ ions on the surface.^{9,24,25} Accordingly, we speculated that the V³⁺ on the (010) and (004) lattice plane could be served as an active sites, benefiting redox reaction from V³⁺ to V⁵⁺ once exposing to oxygen in air. The O 1s components also show their particular binding energies in the spectra (Fig. 4d and Table 1). Especially, the state of O 1s indicates that there are two sorts of oxygen species in the surface, *i.e.*, the lattice oxygen (O_{lattice}) and the adsorbed oxygen (O_{ads}). The former could not be interacted with the reducing gas, and unable to affect the formation of main charge-carrier (electrons) in n-type semiconductor. However, the latter, O_{ads}, readily reacts with the gas and is responsive as a medium.²⁶ Moreover, the integral area of peaks in XPS can be used to quantify the chemical composition because the number of photoelectrons of an element depends on the atomic concentration of these elements in the samples. Thus, with calculating area of the two components, the quantity ratio of V³⁺ / V⁵⁺ (0.1981), O_{ads} / O_{lattice} (0.2581), and O_{ads} / V³⁺ (1.87) were obtained. It reveals that there are a kind of O_{ads} - V³⁺ - O_{ads} structure on the surface of CeVO₄ NRs, and the gas sensing properties may be enhanced since the O_{ads} and V³⁺ play an important role in the gas sensing process as described below.

Growth mechanism of CeVO₄ NRs

Many studies show that the addition of disodium edetate and the alkaline condition have acted a significant impact on the growth of nanocrystals in the reaction system. In our work, Ce(CH₃CO₂)₃, Na₂VO₄ and disodium edetate were inferred to the chelating effect of EDTA on Ce³⁺ ions in alkaline condition.²⁷ These initial CeVO₄ clusters, mediated by the adsorbed ligands on the (010) and (004) crystal planes, could serve as the seeds for the growth of highly anisotropic nanostructures in the solution–solid process (Fig. S2). As the reaction proceeds, the number of generated CeVO₄ clusters gradually increased and began to aggregate under the influence of static electricity or the high surface energy, making the CeVO₄ crystal nuclei grew along a certain direction. Herein, through the analysis of XRD and HRTEM, we know that the growth rate of (101) and (004) lattice planes was inhibited due to the chelation of EDTA, while the (200) lattice plane grew fast. Therefore it is speculated that the growth direction of CeVO₄ clusters was mainly along the (200) lattice plane. Finally, due to the tetragonal zirconia

structure for CeVO₄, the growth rate of (200) lattice plane is faster than the other lattice planes, and the square section for CeVO₄ NRs was reasonably obtained when the hydrothermal reaction was completed. The schematic growth mechanism of CeVO₄ NRs is illustrated in Fig. S2.

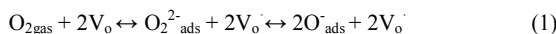
Gas sensing properties and its gas-sensing mechanism

In recent years, environmental pollution and public safety have caused increasing concerns, as a consequent, the alternative gas sensors with excellent performances have become a hot topic because they play an important role in poison gas monitor. In order to demonstrate the potential application in gas sensing, a gas sensor (the inset in Fig. S3) by using the as-prepared CeVO₄ NRs was fabricated. The gas sensor was placed inside the sensing chamber filled with normal atmospheric air, which the resistance of sensors were measured. Subsequently, the test gases were injected into the sensing chamber through a common syringe. Firstly, the selectivity of the as-fabricated CeVO₄ NRs sensor was evaluated by exposing the sensor to different kinds of gases with a concentration of 1000 ppm at an operating voltage 5V. Fig. S3 exhibits a bar graph of the response of the sensor to a variety of gases, such as acetone, hydrogen and methane. The response toward acetone was remarkably higher than that to the other gases. Therefore, it is concluded that the as-fabricated gas sensor showed an excellent selectivity toward acetone. Subsequently, it's well known that the gas response of a gas sensor is highly affected by the varied operating voltages for heating coil inside ceramic tube, hence, the relationships between the operating voltage and gas response of the gas sensor based on CeVO₄ NRs to 1000 ppm acetone were firstly tested. Fig. S4 and Fig. 5a show the response-recovery curves and sensitivity of the gas sensor at different operating voltages, respectively. It can be seen that the responses to acetone varied with the voltage and both of them exhibited an 'increase–maximum–decrease' tendency. At a low operating voltage, acetone molecules cannot effectively react with the surface absorbed oxygen species, which led to a low response. While, with the increasing of voltage, both the higher reaction activity and the conversion of surface absorbed oxygen species (O_{2gas} → O_{2ads} → O_{2-ads} → 2O_{ads}) contributed to the higher response. As the optimum operating voltage further increases, the response reduced because of the low adsorption ability of the acetone molecules, which caused the low response of the sensing materials. Then the 5V operating voltage (Fig. 5a), corresponding a temperature on the surface of sensor, 108 °C (monitored by a FLIR IR (Infrared Radiation) camera player, FLIR company, Germany), was chosen as the optimum operating voltage. Fig. 5b presents the response-recovery curves of the sensor to 1000 ppm acetone at 108 °C. According to the definition of response time and recovery time, the response time to 1000 ppm acetone at 108 °C was about 0.5 s, which presents a rapid response. In the same way, the recovery time to 1000 ppm acetone was about 80 s. Thus, the gas sensor illustrates a relatively rapid response and recovery to acetone. Finally, the response behaviour was further investigated with the exposed to different concentration of acetone at 108 °C for CeVO₄ NRs, and the results are shown in Fig. 6. Apparently, when each 100 ppm acetone was injected into the sensing chamber, the resistances of sensing materials decrease rapidly. As the corresponding linear diagram, the inset in Fig. 6 also shows a good linear relationship between the resistances of the gas sensor and the acetone concentration (100-1000 ppm).

Further, the gas sensing mechanism of CeVO₄ NRs gas sensor (Fig. 7 and S5) is explained according to a surface depletion layer model.^{28,29} At first, as exposure to air atmosphere, oxygen molecules were absorbed into the oxygen vacancies (V_o) on the exposed (010) or (004) lattice planes of CeVO₄ NRs, forming O_{2-ads}, O_{ads} by capturing free electrons from the conduction band of the sensing materials [Eq. (1)], then it results in the decrease of carriers

concentration and the increases of the resistance of gas sensor.³⁰ Meanwhile, trivalent state (V^{3+}) will be oxidized to pentavalent state (V^{5+}) due to the loss of electrons [Eq. (2)]. Later, the gas sensor is exposed to acetone gas, and O_{ads}^- is in favor of adsorbing more acetone molecules, thereby facilitating the subsequent redox reaction, and react with acetone molecules to generate CO_2 and H_2O [Eq. (3)]. It induces that those capturing free electrons return to the sensing materials, $CeVO_4$ NRs, and the resistance reduces reversibly.

In order to further prove the existence of oxygen vacancies of $CeVO_4$ NRs before exposing to O_2 in air, we measured the resistance of the gas sensor in air and infrabar at 300 ppm O_2 (0.003 atm) (Fig. 7). It clearly explains that the corresponding resistance becomes smaller under infrabar (300 ppm O_2) due to the desorption of adsorbed oxygen (O_{ads}) at the active sites, oxygen vacancies (V_o), releasing the electrons to $CeVO_4$ NRs. Further, the resistance of $CeVO_4$ NRs decreases. Once in air, O_2 molecules in air are adsorbed on oxygen vacancies and V^{3+} dangling bonds on the surface. This process is reversible as seen in Fig. 7 and Eq.1-2.



Conclusions

In summary, by using a one step hydrothermal method, we have fabricated the straight and uniform $CeVO_4$ NRs with sectional width ~ 100 nm and length ~ 1.5 μm . During the hydrothermal reaction, the chelation of EDTA on $CeVO_4$ NRs and the control of alkaline conditions played a key role on the grow process of $CeVO_4$ NRs. FE-SEM and TEM observations demonstrated that the appearance of $CeVO_4$ NRs with square section present which mainly due to the tetragonal zircon structure and rapid growth of (200) lattice plane. Due to the presence of V^{3+} active sites (dangling bonds) and oxygen vacancies on the exposed (010) or (004) lattice plane, the gas sensor based on hydrothermally synthesized n-type $CeVO_4$ NRs exhibited highly acetone sensing behaviour at a low operating voltage (108 $^\circ C$), which assumes its novelty for use in medical and other industrial applications. Thus, the acetone gas sensor prepared by $CeVO_4$ NRs will be applied to monitor acetone concentration between 100-1000 ppm with high selectivity. Further efforts will be devoted to the doping effect for $CeVO_4$ NRs in gas sensing behaviour and their dependence on processing conditions.

Acknowledgements

The authors gratefully acknowledge the financial support from National Science Fund of China (NSFC) (21201035, 61201397, J1103303 (J2013-004)), development project of Fujian Provincial Economic and Information Technology Commission (2015-2017), Youth Scientific Research Program of Fujian Provincial Health and Family Planning Commission (2014-1-39), Nursery Scientific Research Foundation of Fujian Medical University (2014MP008), and Fujian Natural Science Foundation (2015J05020).

Notes and references

- 1 L. Adijanto, V. Balaji Padmanabhan, K. J. Holmes, R. J. Gorte and J. M. Vohs, *J. Solid State Chem.*, 2012, **190**, 12.
- 2 R. Jindal, M. M. Sinha and H. C. Gupta, *Spectrochim. Acta, Part A*, 2013, **113**, 286.
- 3 G. Lucovsky and J. Phillips, *Thin Solid Films*, 2005, **486**,

- 4 G. Pagano, F. Aliberti, M. Guida, R. Oral, A. Siciliano, M. Trifuoggi and F. Tommasi, *Environ. Res.*, 2015, **142**, 215.
- 5 G. Li, K. Chao, H. Peng and K. Chen, *Mater. Res. Bull.*, 2008, **112**, 6228.
- 6 M. Oshikiri, J. Ye and M. Boero, *J. Phys. Chem. C*, 2014, **118**, 8331.
- 7 F. Luo, C. Jia, R. Liu, L. Sun and C. Yan, *Mater. Res. Bull.*, 2013, **48**, 1122.
- 8 L. Chen, *Mater. Lett.*, 2006, **60**, 1859.
- 9 S. A. Hakim, Y. Liu, W. Jin, W. Chen, I. Mehmood and V. T. Nguyen, *Mater. Lett.*, 2015, **154**, 144.
- 10 T. Rakshit, S. Santra, I. Manna and S. K. Ray, *RSC Adv.*, 2014, **15**, 947.
- 11 F. Liu, Y. Guan, R. Sun, X. Liang, P. Sun, F. Liu and G. Lu, *Sens. Actuators, B*, 2015, **221**, 673.
- 12 X. Xu, Y. Chen, S. Ma, W. Li and Y. Mao, *Sens. Actuators, B*, 2015, **213**, 222.
- 13 F. Meng, N. Hou, Z. Jin, B. Sun, W. Li, X. Xiao, C. Wang, M. Li and J. Liu, *Sens. Actuators, B*, 2015, **219**, 209.
- 14 S. Liu, F. Zhang, H. Li, T. Chen and Y. Wang, *Sens. Actuators, B*, 2012, **162**, 259.
- 15 J. Do and S. Wang, *Sens. Actuators, B*, 2013, **185**, 39.
- 16 X. Zhou, J. Liu, C. Wang, P. Sun, X. Hu, X. Li, K. Shimanoe, N. Yamazoe and G. Lu, *Sens. Actuators, B*, 2015, **206**, 577.
- 17 Z. Han, J. Wang, L. Liao, H. Pan, S. Shen and J. Chen, *Appl. Surf. Sci.*, 2013, **273**, 349.
- 18 Y. Shen, Y. Huang, S. Zheng, X. Guo, Z. Chen, L. Peng and W. Ding, *Inorg. Chem.*, 2011, **50**, 6189.
- 19 S. Yuvaraj, R. Kalai Selvan, V. B. Kumar, I. Perelshtein, A. Gedanken, S. Isakkimuthu and S. Arumugam, *Ultrason. Sonochem.*, 2014, **21**, 599.
- 20 L. Tan, J. Xu, X. Zhang, Z. Hang, Y. Jia and S. Wang, *Appl. Surf. Sci.*, 2015, **356**, 447.
- 21 D. Guo, C. Hu and Y. Xi, *J. Magn. Alloy.*, 2013, **550**, 389.
- 22 L. Armelao and D. Barreca, *Surf. Sci. Spectra*, 2001, **8**, 247.
- 23 D. Barreca, A. Gasparotto, E. Tondello, C. Sada, S. Polizzi and A. Benedetti, *Chem. Vap. Deposition*, 2003, **9**, 199.
- 24 D. Barreca, L. Depero, V. Noto, G. Rizzi, L. Sangaletti and E. Tondello, *Chem. Mater.*, 1999, **11**, 255.
- 25 V. Raju, J. Rains, C. Gates, W. Luo, X. Wang, W. F. Stickle, G. D. Stucky and X. Ji, *Nano Lett.*, 2014, **14**, 4119.
- 26 H. Zhang, J. Shu, X. Wei, K. Wang and J. Chen, *RSC Adv.*, 2013, **3**, 7403.
- 27 J. Liu, L. Wang, X. Sun and X. Zhu, *Angew. Chem. Int. Ed.*, 2010, **49**, 3492.
- 28 G. Yamamoto, T. Yamashita, K. Matsuo, T. Hyodo and Y. Shimizu, *Sens. Actuators, B*, 2013, **183**, 253.
- 29 J. Khanderi, R. C. Hoffmann, A. Gurlo and J. J. Schneider, *J. Mater. Chem.*, 2009, **19**, 5039.
- 30 X. Han, M. Jin, S. Xie, Q. Kuang, Z. Jiang, Y. Jiang, Z. Xie and L. Zheng, *Angew. Chem. Int. Ed.*, 2009, **48**, 9180.

Figure captions

Fig. 1 XRD pattern of CeVO₄ NRs.

Fig. 2 FE-SEM images (a), (b), (c) and particle size distribution (d) of CeVO₄ NRs.

Fig. 3 TEM images (a) of CeVO₄ NRs, HRTEM images (b) and (c) of CeVO₄ NRs, (the inset is SAED pattern).

Fig. 4 XPS (a) spectra of (b) cerium (Ce 3d), (c) vanadium (V 2p) and (d) oxygen (O 1s) of CeVO₄ NRs.

Fig. 5 Sensitivity (a) of CeVO₄ NRs gas sensor to 1000 ppm acetone gas at different voltages, and its response curve (b) of CeVO₄ NRs gas sensor at 5V (108 °C).

Fig. 6 Response versus acetone concentration of CeVO₄ NRs, and the inset is the corresponding sensitivity curve.

Fig. 7 Response in air and infrabar of CeVO₄ NRs gas sensor at 108 °C, respectively.

Table 1 XPS of Ce 3d, V 2p and O 1s binding energies (eV) for CeVO₄ NRs.

Fig. 1

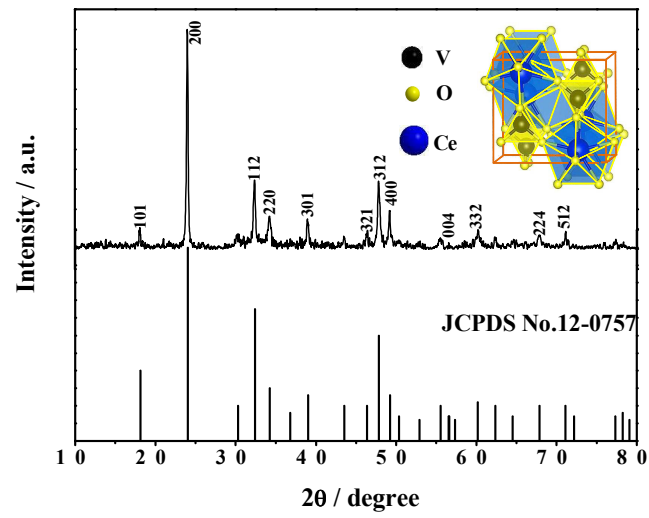


Fig. 2

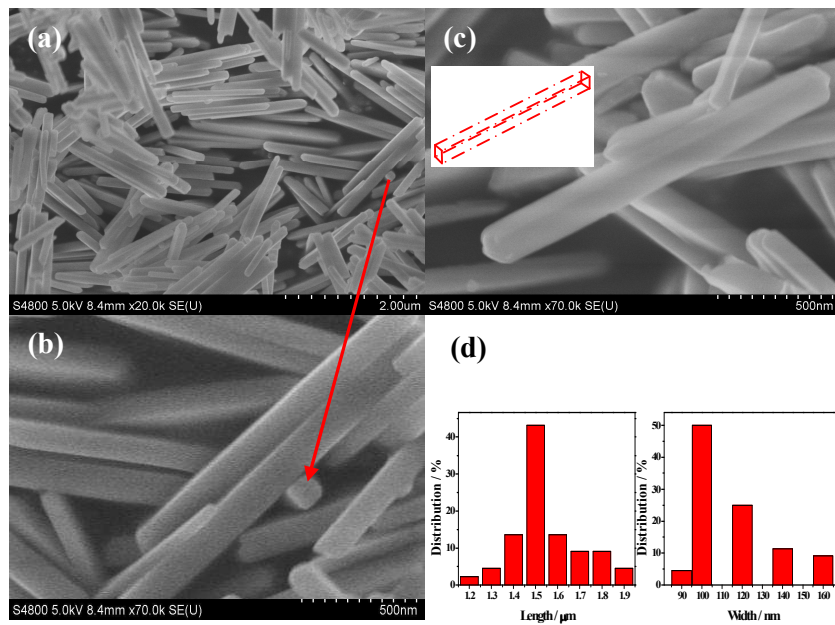


Fig. 3

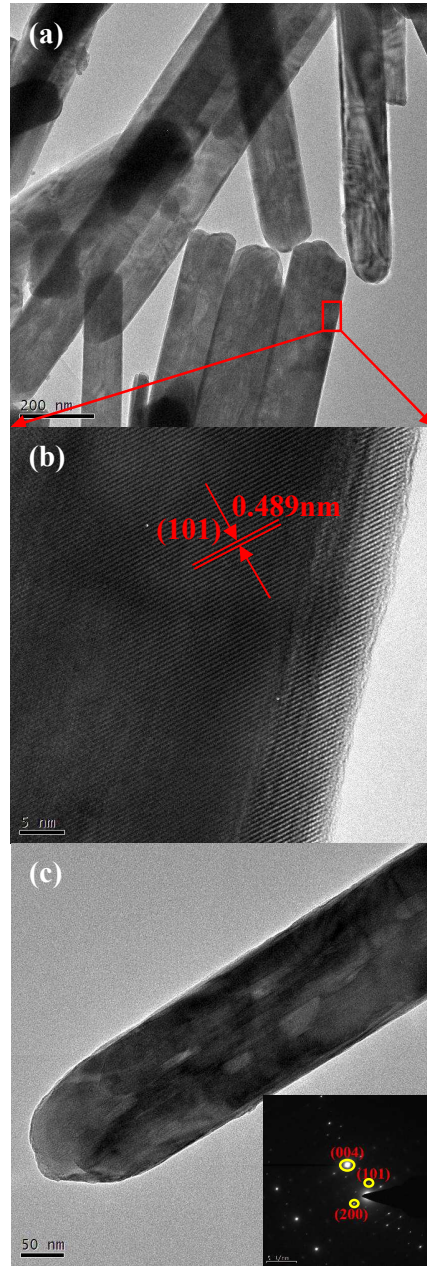


Fig. 4

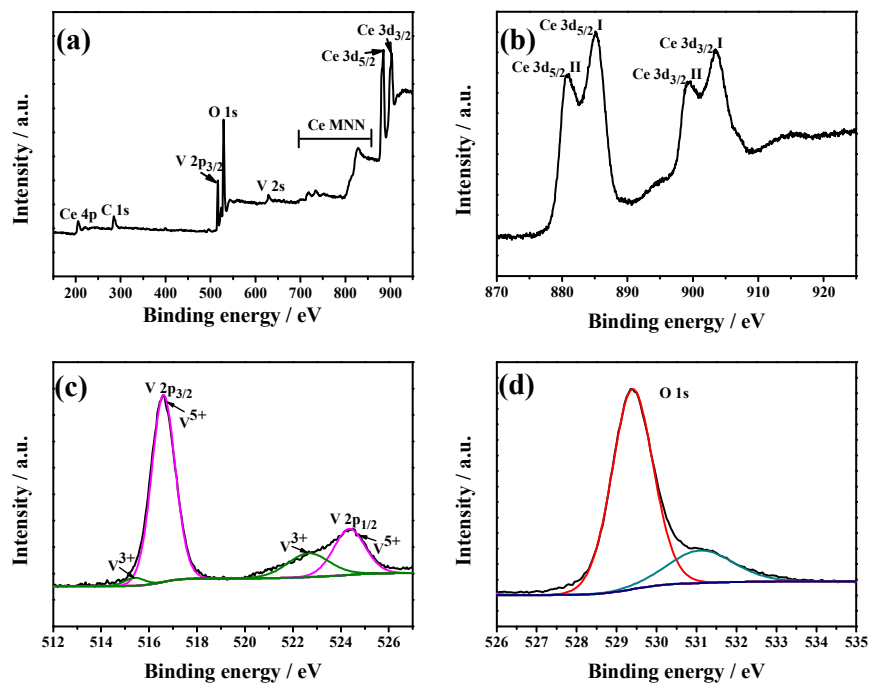


Fig. 5

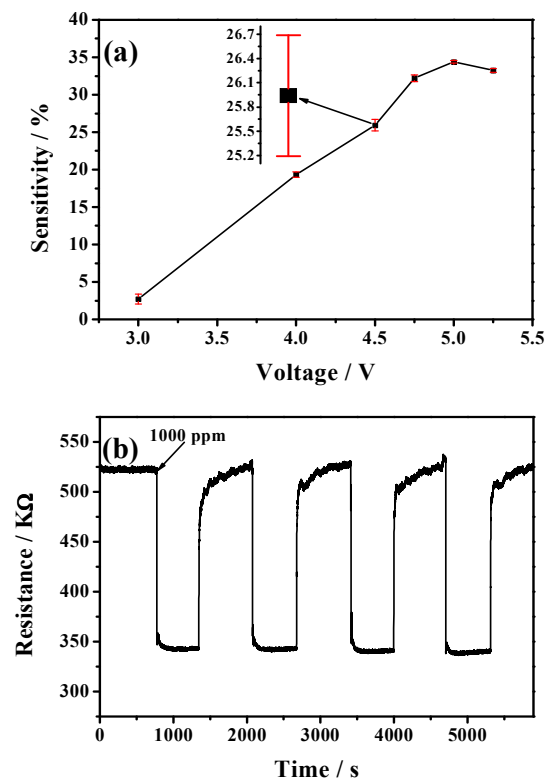


Fig. 6

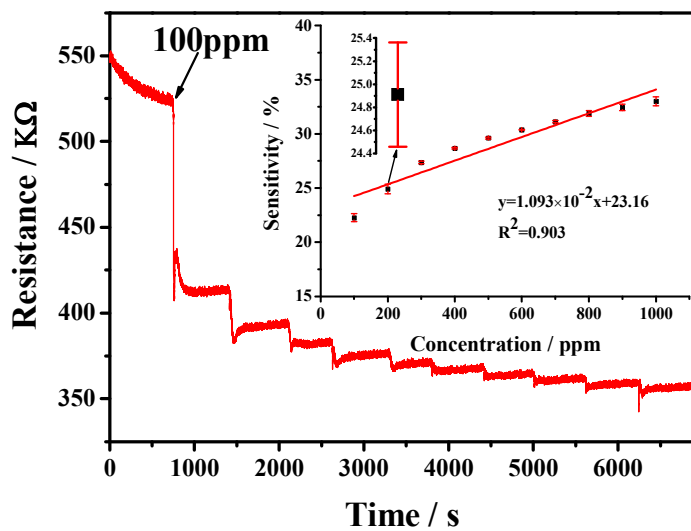


Fig. 7

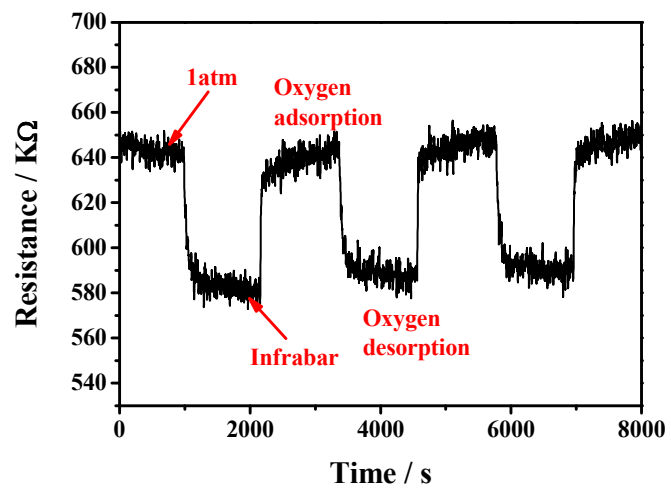
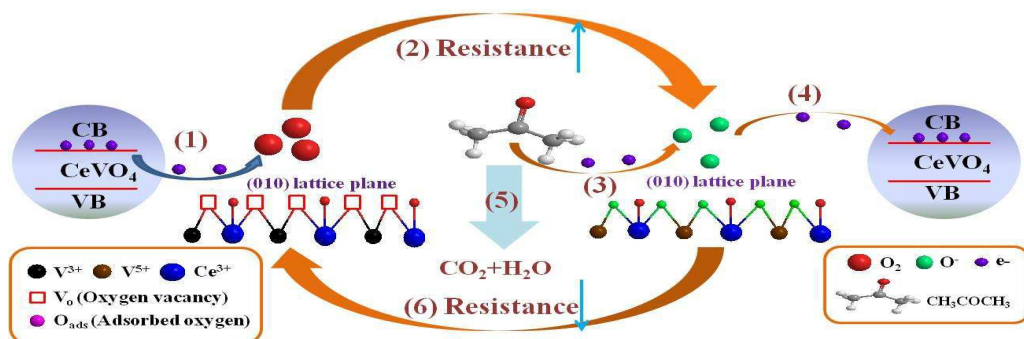


Table 1 XPS of Ce 3d, V 2p and O 1s binding energies (eV) for CeVO₄ NRs.

Phase	Ce 3d		V 2p		O 1s
	3d _{5/2}	3d _{3/2}	2p _{3/2}	2p _{1/2}	
CeVO ₄	880.86 and 885.1	899.5 and 903.3	516.6	524.35	529.4
			515.4	522.65	531.1

Graphical Abstract



The square-section CeVO₄ nanorods with high active and exposed (010) facet were highly promising for acetone gas sensor.